13.2 **DISSIPATION FUNCTION OF WIND SEAS AND WAVE PARAMETERIZATION OF WHITECAP COVERAGE**

Paul A. Hwang* and Mark A. Sletten
Remote Sensing Division, Naval Research Laboratory, 4555 Overlook Ave SW, Washington DC

1. INTRODUCTION

Wind-generated waves are the ocean surface roughness. Mass, momentum and energy passing through the air-sea interface under a given wind condition are modified by surface wave conditions. A useful parameter of wind waves in the study of air-sea exchange is the dissipation function because it quantifies the work done by the wind to the ocean. In many situations detailed wave spectral information is not available, and parameterization of energy dissipation with some global representation of surface waves, such as the significant wave height and dominant wave period, is of great value. In particular, satellite remote sensing using scatterometers, radiometers, altimeters and synthetic aperture radars is now approaching the stage of providing global coverage of wind speed, significant wave height and dominant wave period. A parameterized energy dissipation equation can be used to generate a synoptic estimation of the energy input at the air-sea interface, which is an important upper boundary condition of ocean fluid dynamics.

Source function measurement is one of the most challenging tasks in wind wave research. The dominant source terms of ocean surface waves are wind input, breaking dissipation, and nonlinear wave-wave interaction. Nonlinear interaction exchanges energies between wave spectral components and does not contribute to the overall energy gain or loss of the wave field. The fetch- or duration-limited growth laws can be used to derive a resultant source function, that is, the net growth rate of wind waves [e.g., *Hasselmann et al.*, 1973; *Donelan*, 1998]. Using the independently derived wind generation functions [e.g., *Snyder et al.*, 1981; *Hsiao and Shemdin*, 1983; *Donelan et al*., 2006], the equivalent wind input term can be derived from integrating wind generation function over the whole spectrum. The difference between the integrated wind input and the net wave growth, therefore, represents the integrated energy dissipation. Because net growth rate is only about five percent or less of wind input [*Hasselmann et al.*, 1973; *Donelan*, 1998], for practical purposes, the integrated dissipation function can be approximated with the integrated wind input function. The detailed discussion is presented in Section 2.

In Section 3, the derived dissipation function is applied to whitecap observations that also reported wave measurements. Over the years, extensive observations of whitecaps have led to the conclusion that the power-law wind speed dependence remains the most robust empirical relation describing the whitecap coverage in the ocean despite the consensus that wave parameters somehow play a role because whitecaps are caused by wave breaking, thus it should be related to wave energy dissipation [e.g., *Monahan*, 1971; *Toba and Chaen*, 1973; *Ross and Cardone*, 1974; *Monahan and O'Muircheartaigh*, 1986; *Wu*, 1988; *Zhao and Toba*, 2001; *Lafon et al.*, 2004, 2007; *Anguelova and Webster*, 2006]. With the analytical expression of the integrated dissipation function, it becomes clear that wave energy dissipation is proportional to the cubic power of wind speed and the explicit dependence on wave parameters is $\omega_*^{3.3}\eta_*$, which, for a wide range of wave growth conditions is almost constant. This offers a plausible explanation on why it is so difficult to establish a reliable dependence of whitecap coverage on wave parameters up to this date. A summary is presented in Section 4.

2. DERIVATION OF THE DISSIPATION FUNCTION

2.1. Basic Approach

The energy conservation equation of a wind-generated wave system can be expressed as

$$\frac{dS}{dt} = \langle \gamma \rangle s\omega S \,, \qquad (1)$$

where S is the variance of surface elevation, η_{rms}^2, $<\gamma>$ an average coefficient of energy rate of change, $s=\rho_a/\rho_w$ the ratio of air and water densities, and ω the wave angular frequency. The wave variance is related to the total wave energy per unit area of the ocean surface by $E = \rho_w g H_s^2 / 8 = 2\rho_w g \eta_{rms}^2$, and $H_s = 4\eta_{rms}$ is the significant wave height and g the gravitational acceleration. In the following calculations, s equal to 1/858, which is obtained with ρ_w=1030 kg/m^3 for sea water and ρ_a=1.20 kg/m^3 for air at 20° C [*Beranek*, 1988]. Equation (1) can be applied to wave spectral compo-

*Corresponding author address: Dr. Paul A. Hwang, Naval Research Laboratory, 4555 Overlook Ave SW, Washington DC 20375

nents and further discussion is given in Section 2.2.

In presenting the energy balance equation in the form of (1), it is implied that the wave growth is exponential when $<\gamma>$ is constant. When $<\gamma>$ varies with t, a more general solution is in the form of a power-law (polynomial) function.

Using (1), the energy dissipation of wind waves, $\varepsilon=dE/dt$, can be written in dimensionless form of wind and wave parameters as

$$\varepsilon = 2\rho_a \langle \gamma \rangle \omega_* \eta_* U^3 . \qquad (2)$$

The normalization factors are g and U. In this paper, the neutral wind speed at 10 m elevation, U_{10}, is employed as the reference wind speed. The subscript of wind speed will be dropped for simplicity unless clarification is necessary. Thus $\eta_*=\eta_{rms}^2 g^2/U^4$ and $\omega_*=\omega_p U/g$. The root mean square wave elevation is used in the dimensionless wave variance in order to employ the second-order fitted fetch- and duration-limited growth functions reported by *Hwang and Wang* [2004] and *Hwang* [2006]. They developed a technique to process fetch limited growth data with polynomial functions of the logarithmic of the dimensionless fetch. To the first order the result yields the simple power-law functions. Extending to the second order, the polynomial functions improve the agreement with the data trend considerably, especially for both younger and more mature seas. The fetch-limited growth functions for the first and second order fitting can be written as

$$\eta_* = Ax_*^{\,a}; \quad \omega_* = Bx_*^{\,b}; \eta_* = R\omega_*^{\,r} , \qquad (3)$$

where x is distance (fetch) and $x_*=xg/U^2$. The growth functions have also been converted to the temporal domain to represent duration-limited growth,

$$\eta_* = Pt_*^{\,p}; \quad \omega_* = Qt_*^{\,q} , \qquad (4)$$

where t is time (duration) and $t_*=tg/U$. For the first order fitting, A, a, B, b, P, p, Q, q, R and r are constant. For the second order fitting, they vary with the stage of wave growth, that is, duration, fetch or dimensionless frequency [*Hwang and Wang*, 2004; *Hwang*, 2006]. The computation of the coefficients and exponents for the second order growth functions is somewhat tedious. For convenience, lookup tables with ω_* derived with x_* in logarithmic scale are provided in Table 1.

2.2. Wind Input and Wave Dissipation Functions

Fig. 1a displays field measurements of the wind input coefficient reported by *Snyder et al.* [1981], *Hsiao and Shemdin* [1983] and *Donelan et al.* [2006]. These data are digitized from their Fig. 6, Fig. 4 and Fig. 7, respectively. *Snyder el al.* [1981] and *Donelan et al.* [2006] present their results with a reference wind speed at 5 m elevation, U_5, which is converted to U_{10} using a multiplication factor of 1.06, corresponding to a drag coefficient $C_d=1.2\times10^{-3}$, or equivalently, a dynamic roughness $z_0=10^{-4}$ m, and a logarithmic wind speed profile.

Snyder et al. [1981] suggest that their data can be represented by the following linear function of the ratio between wind speed and wave phase speed, c,

$$\gamma = \frac{1}{s\omega\chi}\frac{d\chi}{dt} \sim (0.2 \text{ to } 0.3)\left(\frac{U_5}{c}-1\right), \qquad (5)$$

where χ is the wave frequency spectrum and γ the growth rate of a spectral component. In Fig. 1a the curve $\gamma=0.25(U_5/c\text{-}1)$ is plotted. The function underpredicts the growth rate at higher U/c region when compared to the measurements of *Hsiao and Shemdin* [1983] but it goes through the middle of the data cluster of *Donelan et al.* [2006].

Hsiao and Shemdin [1983] offer the following function based on the combined data of their own and those of *Snyder et al.* [1981],

$$\gamma = 0.12\left(\frac{U}{c}-1\right)^2 . \qquad (6)$$

The curve lies near the upper bound of the data clusters of *Snyder et al.* [1981] and *Donelan et al.* [2006]. These three sets of field data are combined and least-square power-law fitting yields the following equation based on U/c - 1,

$$\gamma_1 = 0.12\left(\frac{U}{c}-1\right)^{1.7} . \qquad (7)$$

Least square power-law fitting based on U/c produces

$$\gamma_0 = 0.02\left(\frac{U}{c}\right)^{2.7} . \qquad (8)$$

All fitting curves (5) to (8) are shown with the data in Fig. 1a.

To facilitate computation using global wave parameters, an integrated wind input function is defined by

$$<\gamma>=\frac{\int_{\omega_p}^{N\omega_p}\gamma s\omega\chi(\omega)d\omega}{s\omega_p\int_{\omega_p}^{N\omega_p}\chi(\omega)d\omega} . \qquad (9)$$

Spectral analysis of air-sea energy and momentum input shows that the dominant contribution of wind input is from short wave components above the spectral perk frequency [e.g., *Makin et al.*, 1995; *Donelan*, 1998], the integration is carried out from the spectral peak frequency, ω_p, to an upper limit defined by $N\omega_p$

with N>1. The spectral function in this frequency range is assumed to be a power-law function $\chi(\omega) = A_s \omega^{-a_s}$. The detail is described in the Appendix. The quantitative value of the integrated wind input function depends on the assumption of the spectral slope and the frequency bandwidth of integration. Fig. 1b shows the computed $<\gamma>$ as a function of ω_* for two different spectral slopes, -4.1 and -5. (N=5 is used here. In a study of the ocean surface roughness, *Hwang and Wang* [2001] present a discussion suggesting that the frequency bandwidth of the equilibrium range of surface wave spectrum is about $2.5\omega_p$ based on observations of ocean surface mean-square slopes and the consideration of wavenumber components involved in nonlinear wave-wave interaction. The integration here is carried out over a frequency range about twice the equilibrium bandwidth. A sensitivity analysis on the integration frequency bandwidth is presented in the Appendix.) The magnitude of wind input computed with spectral slopes of 4.1 and 5 may differ by a factor of two for either γ_1 or γ_0. The difference between using γ_1 and γ_0 for the same spectral slope appears in the rate of change of $<\gamma>$ with respect to U/c_p; with γ_1, $<\gamma_1>\sim(U/c_p)^2$, and with γ_0, $<\gamma_0>\sim(U/c_p)^{2.7}$. Overall, the average can be approximated by

$$\langle \gamma \rangle = 0.18 \left(\frac{U}{c_p} \right)^{2.3} = 0.18 \omega_*^{2.3} . \qquad (10)$$

The net growth rate of wind generated waves can be estimated from empirical wave growth functions. Using the JONSWAP fetch-limited growth functions, *Hasselmann et al.* [1973] estimate that the net momentum retained in the wave field is about five percent of the wind input. The air-sea momentum flux is calculated with a constant drag coefficient of 0.001. They also perform computation of nonlinear wave-wave interaction using the JONSWAP spectrum. For short fetch conditions, about five percent of momentum flux across the air-sea interface remains in the wave field while more than 90 percent is transferred by wave-wave interaction to shorter waves and then passed to currents through dissipation. For medium to long fetches, they comment that there are ambiguities in the nonlinear interaction computation of the fraction of momentum retained in the wave field.

Donelan [1998] computes the wind input of energy and momentum integrated over the directional spectral function given by *Donelan et al.* [1985] using a growth rate function described by *Donelan and Pierson* [1987]. The net growth rate is computed with the fetch growth laws derived from a field study conducted in Lake Ontario [*Donelan et al*., 1992]. The fraction of energy and momentum retained in the wave field is found to be less than four percent of the total wind input, and a generally decreasing trend toward more mature wave age.

The results from the studies of *Hasselmann et al.* [1973] and *Donelan* [1998] indicate that the net growth rate is only about five percent or less of the wind input. It is therefore justified to approximate the integrated wave dissipation function with the integrated wind input (10) in the present effort seeking to establish a parameterized dissipation function using wind speed and basic wave properties. The energy dissipation of wind waves (2) becomes

$$\varepsilon = \alpha U^3, \text{ with } \alpha = 0.36 \rho_a \omega_*^{3.3} \eta_* U^3 . \qquad (11)$$

Fig. 2a shows the variation of α as a function of wave development, which can be characterized by the dimensionless frequency; note that for deep water wave conditions ω_* is identically the inverse wave age, $1/(c_p/U)$. As wave develops (from large to small ω_*) α gradually increases and reaches a maximum near ω_*=1.8 and then decreases as wave becomes more mature and characteristic roughness decreases. (The characteristic roughness is proportional to $k_p H_s$, where k_p is the wavenumber at the spectral peak. Nonmonotonic behavior of $k_p H_s$ as a function of wave growth has been described by *Hwang* [2005].) This curve can be interpreted as the temporal evolution of wave energy dissipation under forcing by a constant wind speed. Fig. 2b illustrates the temporal evolution of ω_* under duration-limited wave growth for U=5, 10, 15 and 20 m/s. Combining the results of Figs. 2a and 2b, we can obtain the temporal average $<\alpha>$ for different wind speeds of various durations (Fig. 2c). The magnitude of $<\alpha>$ for different durations of wind events is wind speed dependent: from 7×10^{-4} at the young stage to 1.3×10^{-3} at a more mature stage for U=5 m/s, and from 3.5×10^{-4} to 1.3×10^{-3} for U=20 m/s, for example. For common wind events in the ocean with wind duration longer than one hour, the numerical value of α for practical applications is $(0.8 \sim 1.3)\times10^{-3}$.

3. APPLICATION TO WHITECAP OBSERVATIONS

Observations of whitecap coverage on the ocean surface are of great interest because whitecaps are probably the most conveniently observable indication of wave breaking, which plays an important role in air-sea interaction processes and ocean remote sensing applications. Many comprehensive reviews on the subject have been published [e.g., *Monahan and O'Muircheartaigh*, 1986; *Anguelova and Webster*, 2006; and the references therein]. The parameterizations of whitecap coverage, P_w, are usually given as power-law functions of wind speed, some may also

include water temperature and air-sea temperature difference in the parameterization functions. Many attempts to factor in wave parameters, such as wave age or dimensionless fetch, produce formulas that usually fit only selective data sets and it remains uncertain on how to properly account for explicit wave factors in whitecap observations. Fig. 3a shows the whitecap measurements reproduced from the tabulated data of *Monahan* [1971], *Toba and Chaen* [1973], *Ross and Cardone* [1974], *Xu et al.* [2000] and *Lafon et al.* [2004, 2007]; referred to as the MTRXL data set from here on. *Monahan* [1971] suggests that $P_w=1.35\times10^{-5}U^{3.4}$ forms an upper envelop of his whitecap measurements. The envelop function seems to apply to the assembled group of data also. The mean data trend follows very well the semi-analytical function $P_w=1.7\times10^{-6}U^{3.75}$ suggested by *Wu* [1988]. Many more functions with somewhat slightly different coefficients have also been published. A table of 30 is given by *Anguelova and Webster* [2006]. Interestingly, when a threshold wind speed is introduced, a cubic wind speed relation,

$$\begin{aligned} P_w &= 1.5\times10^{-5}\left(U-2\right)^3 \\ &= 1.5\times10^{-5}U^3-1.2\times10^{-4} \end{aligned}, \qquad (12)$$

is found to fit the data equally well or better, especially for the measurements in the lower wind conditions (Fig. 3a). Similar cubic wind speed relationship of whitecap coverage has been proposed by several researchers [e.g., *Bondur and Sharkov*, 1982; *Monahan*, 1993; *Asher and Wanninkhof*, 1998; *Asher et al.*, 2002; *Reising et al.*, 2002; *Stramska and Petelski*, 2003; see Table 1 of *Anguelova and Webster*, 2006].

It is generally agreed that instead of wind speed, the wave energy dissipation is a better parameter to interpret the whitecap data because whitecaps are generated by breaking waves [e.g., *Toba and Chaen*, 1973; *Ross and Cardone*, 1974; *Monahan and O'Muircheartaigh*, 1986; *Wu*, 1988; *Zhao and Toba*, 2001]. Out of the 200 data points in MTRXL, 79 are accompanied with the report of significant wave height and peak wave frequency to facilitate dissipation computation as described in the last section. The result is shown in Fig. 3b and the data can be represented by the power-law function

$$P_w = 8.5\times10^{-3}\left(\varepsilon-\varepsilon_c\right). \qquad (13)$$

The threshold energy dissipation for whitecap inception, ε_c, is between 0.02 and 0.06 W/m^2 judging from the data fitting. *Ross and Cardone* [1974] suggest a similar linear dependence between P_w and ε but the intercept of the linear function is positive ($P_w=8.93\times10^{-3}\varepsilon+1.85\times10^{-4}$); that is, the threshold value of energy dissipation in their equation is negative. Their equation is also show in Fig. 3b for comparison.

The explicit wave properties are embedded in the α factor. As discussed in the last section and illustrated in Fig. 2a, the numerical value of α is relatively unchanged over a broad range of wave development conditions (within a factor of about 1.3 for the range of ω_*, between 1 and 3, in the data of MTRXL that are accompanied with wave measurements; see Fig. 4 later), and the influence is too weak to be clearly identified due to the large scatter of whitecap measurements (typically one order of magnitude at a given wind speed). Fig. 4a displays P_w/U^3 to remove the strong cubic wind speed dependence, as suggested by (12) and (13), in order to explore the dependence of whitecap coverage on wave parameters. Data of P_w/U^3 seem to show a local peak near $\omega_*=1.6$, the trend is independent of wind speed as suggested by the plots of subgroups dividing the MTRXL data set into three wind speed bins. Although the scatter is large, the resemblance of the local maximum of P_w/U^3 and that of α (near $\omega_*=1.8$) is encouraging in confirming a correlation between whitecap coverage and surface wave energy dissipation. Furthermore, because α is relatively constant, a cubic power-law wind speed function (12) is equally robust for describing the whitecap coverage in the ocean (Fig. 3).

The data trend shown in Fig. 3b suggests that there is a threshold dissipation level for whitecap inception; the numerical value of the threshold is between 0.02 and 0.06 W/m^2. (The uncertainty in the proposed threshold value is due to the consideration that several low wind data points in Fig. 3a do not have wave measurements for energy dissipation computation.) Substituting this value into the energy dissipation equation (11), the critical wind speed for whitecap inception as a function of wave development stage can be computed (Fig. 4b). The variation of the critical wind speed is relatively insensitive to the stage of wave growth in the ω_* range between 1 and 4. The minimal critical wind speed is about 2.5 to 3.6 m/s and occurs near $\omega_*=1.8$. This is in good agreement with the review by *Monahan and O'Muircheartaigh* [1986], who summarize in their abstract that "The wind speed associated with the onset of whitecapping, while also varying with ΔT and T_w, is typically 3 to 3.5 m s^{-1}, not the often quoted 7 m s^{-1}." (ΔT and T_w are air-sea temperature difference and water temperature, respectively.) Whitecaps do occur under conditions with wind speed less than 3 m/s (see Fig. 3a).

Summarizing the above discussions, it becomes obvious that there is an apparent discrepancy of the threshold values used in the whitecap equations based on wind speed (12) and energy dissipation (13). It is quite likely that at lower wind conditions, other envi-

ronmental factors modify the generation of wind waves, causing the wave field to deviate from that predicted by the fetch- or duration-limited growth laws. The calculation of energy dissipation using (2) is therefore subject to larger uncertainty for low wind conditions.

4. SUMMARY

Using the robust fetch- or duration-limited growth functions of wind-generated waves, the net growth rate of surface waves has been shown to be about five percent or less of the integrated wind input [*Hasselmann et al.*, 1973; *Donelan*, 1998]. The integrated dissipation function can therefore be approximated by the integrated wind input function. An analytical expression of the wind input and dissipation function is derived: $\varepsilon = \alpha U^3$ with $\alpha = 0.36\rho_a \omega_*^{3.3}\eta_*$. Based on this equation, the energy dissipation of surface waves per unit area of the ocean surface is proportional to the cubic power of wind speed and the explicit dependence of wave parameters is $\omega_*^{3.3}\eta_*$ (Fig. 2a). Satellite remote sensing is now capable of providing global coverage of wind speed, significant wave height and dominant wave period. A parameterization equation such as the one given above can be used to generate a first-order estimation of the surface wave energy dissipation in the world's oceans. The surface wave energy dissipation represents the energy input from atmosphere to ocean and is an important upper boundary condition for the study of ocean fluid dynamics.

Applying the energy dissipation calculation to whitecap data that also reported wave measurements, the whitecap coverage as a function of surface wave energy dissipation is found to be P_w=8.5×10^{-3}(ε-ε_c) with ε_c is between 0.02 and 0.06 W/m^2. For a wide range of wave development conditions, α is almost constant. This may explain why it is very difficult to detect the dependence of whitecap coverage on explicit wave parameters. The MTRXL data used for energy dissipation analysis in this paper can be described equally well by P_w=1.5×10^{-5}(U-2)^3 (Fig. 3).

ACKNOWLEDGEMENTS

This work is supported by the Office of Naval Research (NRL Work Unit 6683 and 8953, and Program Element N61153 and N62435, NRL contribution number NRL/PP/7260—07-xxxx).

APPENDIX. NUMERICAL COMPUTATION OF WIND INPUT FUNCTION

The wind input function derived from field measurements [e.g., *Snyder et al.*, 1981; *Hsiao and Shemdin*, 1983; *Donelan et al.*, 2006] is for individual wave components. The net growth rate obtained from fetch- or duration-limited growth laws represents the result integrated over the full wave spectrum. In order to compare the two functions, an integrated wind input function is calculated by

$$<\gamma>=\frac{\int_{\omega_p}^{N\omega_p}\gamma s\omega\chi(\omega)d\omega}{s\omega_p\int_{\omega_p}^{N\omega_p}\chi(\omega)d\omega}. \qquad \text{(A1)}$$

Expressing the spectral function in the high frequency range above the spectral peak as $\chi(\omega)=A_s\omega^{-a_s}$, and denoting σ=U/c=$\omega U/g$, then for $\gamma_0 = B_0\sigma^{b_0}$, (A1) becomes

$$<\gamma_0>=\gamma_{0p}\frac{(1-a_s)\left(N^{b_0+2-a_s}-1\right)}{\left(N^{1-a_s}-1\right)(b_0+2-a_s)}, \qquad \text{(A2)}$$

where $\gamma_{0p} = B_0\sigma_p^{b_0}$, note that σ_p and ω_* are identical.

For $\gamma_1 = B_1(\sigma-1)^{b_1}$ and an arbitrary b_1, the integration in the numerator of (A1) results in a solution in terms of the Gauss hypergeometric function. The numerical evaluation of the solution is rather cumbersome. Based on the experimental data, b_1 is 1.7 (Eq. 7), which is between 1 and 2. Because simple solutions are available for b_1=1 and 2, the computation presented here is interpolated from the two particular solutions. Denoting $<\gamma_1>_1$ as the integrated wind input function for b_1=1 and $<\gamma_1>_2$ for b_1=2, then

$$<\gamma_1>_1=\gamma_{1p}\frac{(1-a_s)}{\left(N^{1-a_s}-1\right)}\left[\frac{N^{3-a_s}-1}{3-a_s}\sigma_p^2-\frac{N^{2-a_s}-1}{2-a_s}\sigma_p\right] \qquad \text{(A3)}$$

$$<\gamma_1>_2=\gamma_{1p}\frac{(1-a_s)}{\left(N^{1-a_s}-1\right)}\left[\frac{N^{4-a_s}-1}{4-a_s}\sigma_p^3-2\frac{N^{3-a_s}-1}{3-a_s}\sigma_p^2+\frac{N^{2-a_s}-1}{2-a_s}\sigma_p\right] \qquad \text{(A4)}$$

where $\gamma_{1p} = B_1(\sigma_p-1)^{b_1}$.

Solutions (A3) and (A4) can be easily evaluated for a_s not equal to 1, 2, 3 or 4. Examples of computational results are shown in Fig. A1 for a_s=4.1 and 5. In (a), $<\gamma_0>$ and $<\gamma_1>$ computed for N=5, 10 and 20 are graphed. The sensitivity to the frequency bandwidth of integration is shown in (b). The wider the integration frequency bandwidth, the larger the numerical value of the proportionality coefficient of the dissipation rate. A better understanding of the physics of wave generation and dissipation will help in defining a more accurate value for the frequency range of integration.

REFERENCES

Anguelova, M. D., and F. Webster, 2006: Whitecap coverage from satellite measurements: A first step toward modeling the variability of oceanic whitecaps. *J. Geophys. Res.*, *111*, C03017, doi:10.1029/2005JC003158.

Asher, W., and R. Wanninkhof, 1998: The effect of bubble-mediated gas transfer on purposeful dual-gaseous tracer experiment. *J. Geophys. Res.*, *103*, 10555-10560.

Asher, W., J. Edson, W. McGillis, R. Wanninkhof, D. Ho, and T, Litchendorf, 2002: Fractional area whitecap coverage and air-sea gas transfer velocities measured during GasEx-98, in *Gas Transfer at Water Surfaces, Geophys. Monogr. Ser.*, vol. 127, edited by M. Donelan et al., pp. 199-204, AGU, Washington DC.

Beranek, L. L., 1988: *Acoustic measurements*, American Institute of Physics, Cambridge, MA, 841 pp.

Bondur, V., and E. Sharkov, 1982: Statistical properties of whitecaps on a rough sea, *Oceanology, 22*, 961-963.

Donelan, M. A., 1998: Air-water exchange processes, in *Physical Processes in Lakes and Oceans*, ed. J. Imberger, Coastal and Estuarine Studies Volume 54, 19-36, American Geophysical Union.

Donelan, M. A., and W. J. Pierson, 1987: Radar scattering and equilibrium ranges in wind-generated waves with application to scatterometry, *J. Geophys. Res.*, *92*, 4971-5029.

Donelan, M. A., J. Hamilton, and W. H. Hui, 1985: Directional spectra of wind-generated waves, *Phil. Trans. Roy. Soc. Lond.*, *A315*, 509-562.

Donelan, M. A., M. Skafel, H. Graber, P. Liu, D. Schwab, and S. Venkatesh, 1992: On the growth rate of wind-generated waves, *Atmos.-Ocean, 30*, 457-4782.

Donelan, M. A., A. V. Babanin, I. R. Young, and M. L. Banner, 2006: Wave-follower field measurements of the wind-input spectral function. Part II: Parameterization of the wind input, *J. Phys. Oceanogr., 36*, 1672-1689.

Hasselmann, K. et al., 1973: Measurements of wind-wave growth and swell decay during the Joint North Sea Wave Project (JONSWAP), *Dtsch. Hydrogr. Z., Suppl. A, 8(12)*, 95pp.

Hsiao, S. V., and O. H. Shemdin, 1983: Measurements of wind velocity and pressure with a wave follower during MARSEN, *J. Geophys. Res., 88*, 9841-9849.

Hwang, P. A., 2005: Drag coefficient, dynamic roughness and reference wind speed, *J. Oceanogr., 61*, 399-413.

Hwang, P. A., 2006: Duration- and fetch-limited growth functions of wind-generated waves parameterized with three different scaling wind velocities, *J. Geophys. Res., 111*, C02005, doi:10.1029/2005JC003180.

Hwang, P. A., and D. W. Wang, 2001: Directional distributions and mean square slopes in the equilibrium and saturation ranges of the wave spectrum, *J. Phys. Oceanogr., 31*, 1346-1360.

Hwang, P. A., and D. W. Wang, 2004: Field measurements of duration limited growth of wind-generated ocean surface waves at young stage of development, *J. Phys. Oceanogr., 34*, 2316-2326. (Corrigendum, *35*, 268-270, 2005).

Lafon, C., J. Piazzola, P. Forget, O. Le Calve, and S. Despiau, 2004: Analysis of the variations of the whitecap fraction as measured in a coastal zone, *Bound.-Layer Meteorol., 111*, 339-360.

Lafon, C., J. Piazzola, P. Forget, and S. Despiau, 2007: Whitecap coverage in coastal environment for steady and unsteady wave field conditions, *J. Mar. Syst.*, doi:10.1016/j.jmarsys.2006.02.013 (in press).

Makin, V. K., V. N. Kudryavtsev, and C. Mastenbroek, 1995: Drag on the sea surface, *Bound. Layer Meteorol. 73*, 159-182.

Monahan, E. C., 1971: Oceanic whitecaps, *J. Phys. Oceanogr., 1*, 139-144.

Monahan, E. C., 1993: Occurrence and evolution of acoustically relevant subsurface bubble plumes and their associated, remotely monitorable, surface whitecaps, in *Natural Physical Sources of Underwater Sound*, ed. B. Kerman, pp. 503-507, Springer, New York.

Monahan, E. C., and I. G. O'Muircheartaigh, 1986: Whitecaps and the passive remote sensing of the ocean surface, *Int. J. Remote Sensing., 7*, 627-642.

Reising, S., W. Asher, L. Rose, and M. Aziz, 2002: Passive polarimetric remote sensing of th ocean surface: The effects of surface roughness and whitecaps, paper presented at the International Union of Radio Science, Maastricht, Netherlands.

Ross, D. B., and V. Cardone, 1974: Observations of oceanic whitecaps and their relation to remote measurements of surface wind stress, *J. Geophys. Res., 79*, 444-452.

Snyder, R. L., F. W. Dobson, J. A. Elliot, and R. B. Long, 1981: Array measurement of atmospheric pressure fluctuations above surface gravity waves, *J. Fluid Mech., 102*, 1-59.

Stramska, M., and T. Petelski, 2003: Observations of oceanic whitecaps in the north polar waters of the Atlantic, *J. Geophys. Res., 108*, C33086, doi:10.1029/2002JC001321.

Toba, Y., and M. Chaen, 1973: Quantitative expression of the breaking of wind waves on the sea surface, *Records Oceanogr. Works Japan, 12*, 1-11.

Wu, J., 1988: Variations of whitecap coverage with wind stress and water temperature, *J. Phys. Oceanogr., 18*, 1448-1453.

Xu, D., X. Liu, and D. Yu, 2000: Probability of wave breaking and whitecap coverage in a fetch-limited sea, *J. Geophys. Res., 105*, 14253-14259.

Zhao, D., and Y. Toba, 2001: Dependence of whitecap coverage on wind and wind-wave properties, *J. Oceanogr., 57*, 603-616.

TABLE 1. LOOKUP TABLES FOR THE FETCH- AND DURATION-LIMITED GROWTH FUNCTIONS

(a) Fetch-limited

ω_*	A	a	B	b	$100R$	r	η_*
20.857	2.236e-8	1.765	20.857	-0.399	1.527	-4.422	2.236e-8
17.397	2.267e-8	1.705	20.809	-0.389	1.365	-4.384	4.972e-8
14.578	2.363e-8	1.645	20.663	-0.379	1.222	-4.344	1.075e-7
12.274	2.530e-8	1.586	20.424	-0.369	1.095	-4.302	2.263e-7
10.382	2.785e-8	1.526	20.093	-0.358	0.983	-4.257	4.632e-7
8.822	3.152e-8	1.467	19.676	-0.348	0.883	-4.210	9.227e-7
7.532	3.665e-8	1.407	19.177	-0.338	0.795	-4.160	1.788e-6
6.461	4.381e-8	1.347	18.604	-0.328	0.717	-4.107	3.372e-6
5.568	5.382e-8	1.288	17.965	-0.318	0.648	-4.050	6.185e-6
4.821	6.796e-8	1.228	17.266	-0.308	0.587	-3.990	1.104e-5
4.193	8.820e-8	1.169	16.517	-0.298	0.533	-3.926	1.917e-5
3.665	1.177e-7	1.109	15.728	-0.288	0.485	-3.857	3.239e-5
3.218	1.613e-7	1.049	14.906	-0.277	0.443	-3.783	5.324e-5
2.838	2.273e-7	0.990	14.062	-0.267	0.405	-3.703	8.515e-5
2.516	3.293e-7	0.930	13.203	-0.257	0.373	-3.617	1.325e-4
2.240	4.902e-7	0.871	12.340	-0.247	0.344	-3.524	2.006e-4
2.004	7.500e-7	0.811	11.479	-0.237	0.319	-3.424	2.954e-4
1.801	1.180e-6	0.751	10.628	-0.227	0.297	-3.314	4.233e-4
1.626	1.907e-6	0.692	9.795	-0.217	0.279	-3.194	5.902e-4
1.475	3.168e-6	0.632	8.985	-0.207	0.263	-3.062	8.006e-4
1.344	5.410e-6	0.573	8.204	-0.196	0.250	-2.916	1.057e-3
1.231	9.495e-6	0.513	7.455	-0.186	0.241	-2.755	1.357e-3
1.132	1.713e-5	0.454	6.744	-0.176	0.233	-2.575	1.695e-3
1.047	3.176e-5	0.394	6.072	-0.166	0.230	-2.373	2.060e-3
0.972	6.053e-5	0.334	5.441	-0.156	0.229	-2.145	2.436e-3
0.907	1.186e-4	0.275	4.853	-0.146	0.233	-1.885	2.803e-3
0.850	2.387e-4	0.215	4.309	-0.136	0.242	-1.587	3.138e-3
0.800	4.940e-4	0.156	3.808	-0.125	0.259	-1.240	3.417e-3
0.757	1.051e-3	0.096	3.349	-0.115	0.287	-0.832	3.621e-3
0.720	2.297e-3	0.036	2.932	-0.105	0.333	-0.346	3.733e-3
0.687	5.161e-3	-0.023	2.555	-0.095	0.410	0.244	3.744e-3

(b) Duration-limited

ω_*	P	p	Q	q	$100R$	r	η_*
20.857	4.558e-14	2.936	403.734	-0.664	1.527	-4.422	2.236e-8
17.397	9.357e-14	2.790	351.845	-0.636	1.365	-4.384	4.972e-8
14.578	1.945e-13	2.648	305.917	-0.610	1.222	-4.344	1.075e-7
12.274	4.091e-13	2.511	265.395	-0.584	1.095	-4.302	2.263e-7
10.382	8.705e-13	2.379	229.751	-0.559	0.983	-4.257	4.632e-7
8.822	1.873e-12	2.250	198.487	-0.535	0.883	-4.210	9.227e-7
7.532	4.071e-12	2.126	171.140	-0.511	0.795	-4.160	1.788e-6
6.461	8.942e-12	2.005	147.282	-0.488	0.717	-4.107	3.372e-6
5.568	1.983e-11	1.888	126.519	-0.466	0.648	-4.050	6.185e-6
4.821	4.440e-11	1.774	108.493	-0.445	0.587	-3.990	1.104e-5
4.193	1.003e-10	1.664	92.877	-0.424	0.533	-3.926	1.917e-5
3.665	2.287e-10	1.557	79.380	-0.404	0.485	-3.857	3.239e-5
3.218	5.256e-10	1.452	67.737	-0.384	0.443	-3.783	5.324e-5
2.838	1.218e-09	1.351	57.714	-0.365	0.405	-3.703	8.515e-5
2.516	2.845e-09	1.252	49.102	-0.346	0.373	-3.617	1.325e-4
2.240	6.697e-09	1.156	41.716	-0.328	0.344	-3.524	2.006e-4
2.004	1.588e-08	1.063	35.393	-0.310	0.319	-3.424	2.954e-4
1.801	3.792e-08	0.972	29.988	-0.293	0.297	-3.314	4.233e-4
1.626	9.119e-08	0.883	25.376	-0.277	0.279	-3.194	5.902e-4
1.475	2.207e-07	0.797	21.447	-0.260	0.263	-3.062	8.006e-4
1.344	5.378e-07	0.713	18.104	-0.244	0.250	-2.916	1.057e-3

```
1.231 1.318e-06   0.631  15.265  -0.229   0.241  -2.755 1.357e-3
1.132 3.252e-06   0.550  12.856  -0.214   0.233  -2.575 1.695e-3
1.047 8.068e-06   0.472  10.816  -0.199   0.230  -2.373 2.060e-3
0.972 2.013e-05   0.396   9.090  -0.185   0.229  -2.145 2.436e-3
0.907 5.051e-05   0.322   7.631  -0.171   0.233  -1.885 2.803e-3
0.850 1.274e-04   0.249   6.401  -0.157   0.242  -1.587 3.138e-3
0.800 3.231e-04   0.178   5.363  -0.143   0.259  -1.240 3.417e-3
0.757 8.234e-04   0.108   4.489  -0.130   0.287  -0.832 3.621e-3
0.720 2.109e-03   0.041   3.755  -0.118   0.333  -0.346 3.733e-3
0.687 5.427e-03  -0.026   3.138  -0.105   0.410   0.244 3.744e-3
```

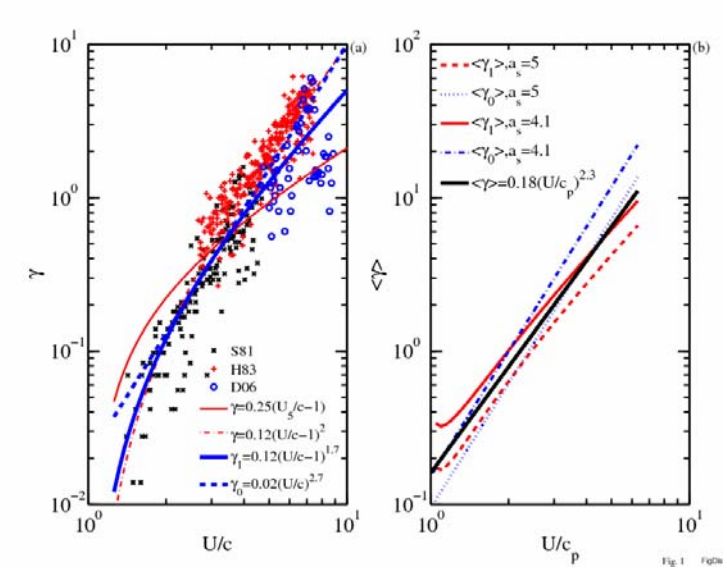

Fig. 1. (a) Wind input data obtained from field environments [*Snyder et al.*, 1981; *Hsiao and Shemdin*, 1983; *Donelan et al.*, 2006]. Also shown are the fitting functions proposed by the individual authors and from least-square fitting of the combined data. (b) The integrated wind input coefficient computed with different spectral slopes and fitting functions of wind input coefficient.

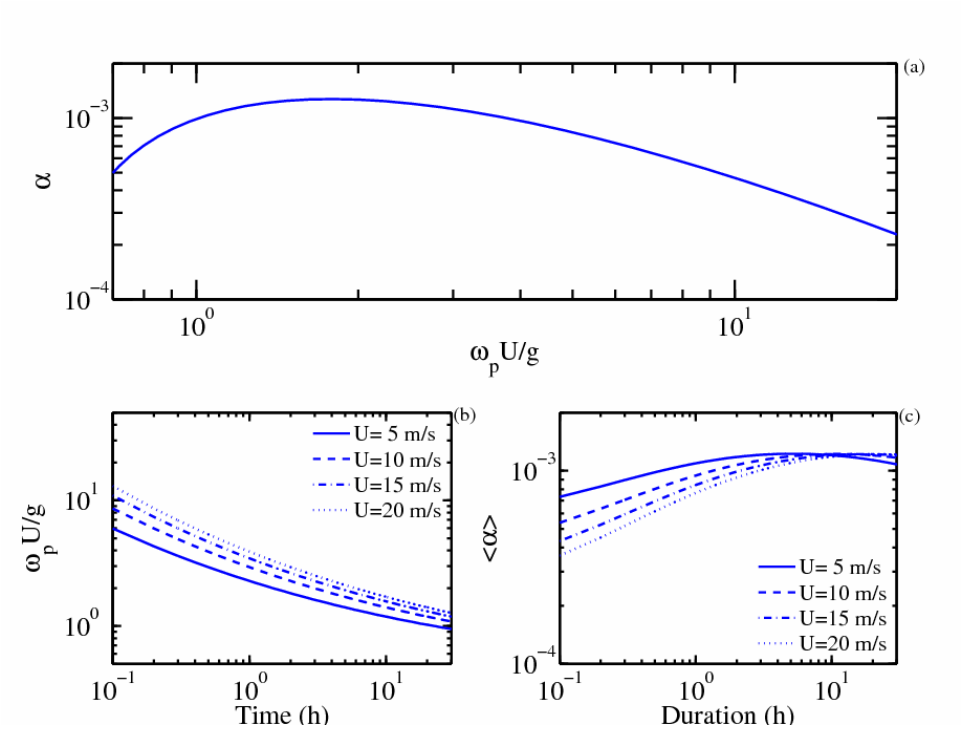

Fig. 2. (a) Dependence of the proportionality coefficient of the dissipation function on the dimensionless frequency. (b) The temporal variation of the dimensionless frequency of duration-limited wave growth. (c) The proportionality coefficient averaged over the duration of wind event plotted as a function of the wind event duration.

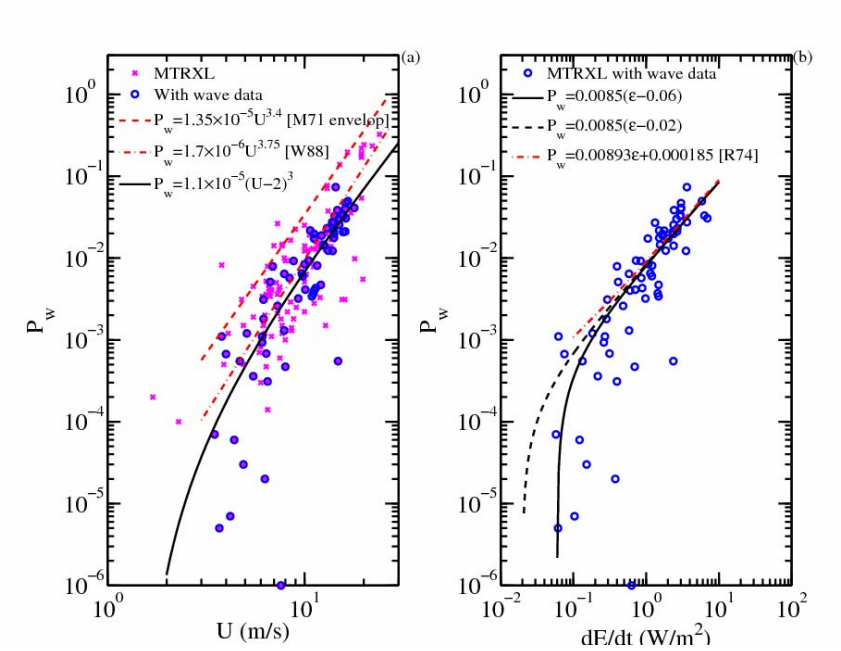

Fig. 3. (a) Wind speed dependence of whitecap observations reproduced from the tables in MTRXL [*Monahan*, 1971; *Toba and Chaen*, 1973; *Ross and Cardone*, 1974; *Xu et al.*, 2000; *Lafon et al.*, 2004, 2007]. (b) The dependence of whitecap coverage on surface wave energy dissipation.

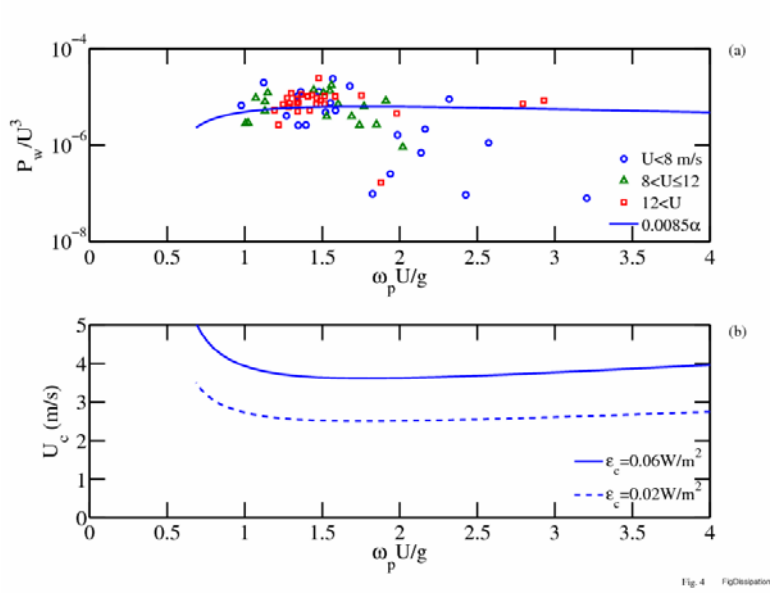

Fig. 4. (a) Dependence of whitecap coverage on wave parameters after the explicit wind speed dependence is removed. (b) The critical wind speed at whitecap inception estimated from the observed apparent energy dissipation threshold.

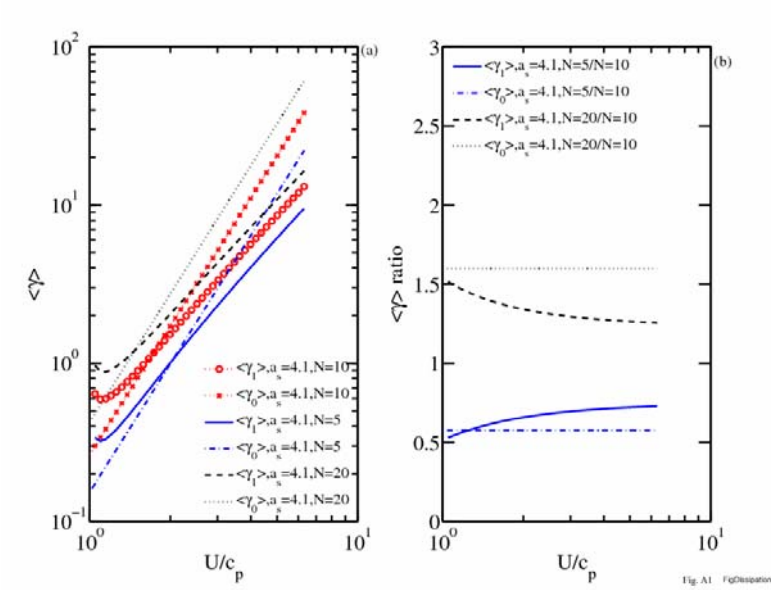

Fig. A1. (a) Examples of the integrated wind input function computed with different fitting functions and spectral frequency bandwidths (represented by *N*). (b) The ratio of integrated wind input function computed with different spectral frequency bandwidths, with N=10 as reference.